INTERNATIONAL JOURNAL FOR NUMERICAL METHODS IN FLUIDS, VOL. 11, 405–426 (1990)

NON-OSCILLATORY SHOCK-CAPTURING FINITE ELEMENT METHODS FOR THE ONE-DIMENSIONAL COMPRESSIBLE EULER EQUATIONS

J. Y. YANG, FUE-SANG LIEN AND CHANG-AN HSU

Institute of Applied Mechanics, National Taiwan University, Taipei 10764, Taiwan, R.O.C.

SUMMARY

A class of shock-capturing Petrov–Galerkin finite element methods that use high-order non-oscillatory interpolations is presented for the one-dimensional compressible Euler equations. Modified eigenvalues which employ total variation diminishing (TVD), total variation bounded (TVB) and essentially non-oscillatory (ENO) mechanisms are introduced into the weighting functions. A one-pass Euler explicit transient algorithm with lumped mass matrix is used to integrate the equations. Numerical experiments with Burgers' equation, the Riemann problem and the two-blast-wave interaction problem are presented. Results indicate that accurate solutions in smooth regions and sharp and non-oscillatory solutions at discontinuities are obtainable even for strong shocks.

KEY WORDS TVD TVB ENO Finite element Euler equations

INTRODUCTION

In recent years the development of the finite element methodology for the first-order hyperbolic system of conservation laws has become an active area of research. The earlier finite element developments include those of Wahlbin,[1] Dendy[2] and Raymond and Garder[3] for first-order hyperbolic equations. Hughes and Tezduyar[4] generalized the streamline upwind/Petrov–Galerkin procedure to hyperbolic conservation laws for one- and multidimensional problems. Donea[5] developed the Taylor–Galerkin algorithm in which the weak statement was formed on a Taylor series expansion of the unsteady equation, with higher-order derivatives re-expressed in terms of derivatives of the flux vector of the hyperbolic conservation laws. Baker and Kim[6] generalized these concepts and proposed a Galerkin weak-statement formulation which encompasses over a dozen independently derived finite difference and finite element dissipative algorithms. Oden *et al.*[7] used a semi-explicit two-step algorithm for the analysis of unsteady inviscid compressible flow in arbitrary two-dimensional domains.

However, in many cases, Gibbs-type oscillations of the solutions can still be observed owing to the presence of discontinuities, which are the main difficulty in the numerical solution of first-order hyperbolic conservation laws. An artificial viscosity or a limiter function is needed to control such oscillatory behaviour.

Harten[8] developed the concept of TVD (total variation diminishing) and constructed second-order shock-capturing schemes using finite difference methods which have proved to be very successful in solving the compressible Euler equations for high-speed flows.[9–13] Many desirable

0271–2091/90/120405–22$11.00

Received 8 December 1989

properties of TVD schemes, such as stability and robustness in solving the hyperbolic conservation laws with strong shocks, have been demonstrated.

One characteristic of TVD schemes is that they are at most first-order accurate at non-sonic critical points. This restricts the accuracy of TVD schemes to be at most first-order in the L_∞-norm and at most second-order in the L_1-norm for general problems.

To overcome this difficulty, Harten and Osher[14] and Harten *et al.*[15,16] have constructed ENO (essentially non-oscillatory) schemes which use a local adaptive stencil to obtain information automatically from regions of smoothness when the solution develops discontinuities. As a result, approximations using these methods can achieve uniformly high-order accuracy right up to discontinuities, while keeping a sharp, essentially non-oscillatory shock transition. However, a convergence theory for ENO schemes is still not available at the present time.

Numerical experiments on ENO schemes for the scalar conservation law in two dimensions and the Euler equation in one dimension have been reported.[14–16] Also, results for two-dimensional gas-dynamic problems involving multiple-shock interactions have been given in Reference 17.

In Reference 18 a class of TVB (total variation bounded) uniformly high-order schemes has been proposed for the hyperbolic conservation laws by Shu and Osher, which they claim share most of the advantages and may remove local degeneracy at the critical points of TVD schemes.

The TVD, TVB and ENO concepts and the resulting so-called high-resolution schemes are mostly developed in the finite difference or finite volume setting.

Hughes and Mallet[19] first translated the idea of TVD flux limiter functions from Roe[20,21] and Sweby[9] into the finite element method. They introduced a similar limiter function in the weighting function which multiplies the time derivative term in the variational equations. A two-pass predictor–corrector explicit scheme was used for the time integration. High-precision results which match the quality of those obtained using finite difference methods were observed. Also, characteristic Galerkin methods for hyperbolic problems have been developed by Morton.[22] Adaptive finite element shock-capturing schemes using a flux-corrected transport algorithm have been developed and applied to transient shock interaction problems.[23,24] Most recently, a class of TVB discontinuous Galerkin finite element methods using high-order TVD Runge–Kutta-type time discretizations has been developed for the one-dimensional Euler equations.[25]

In this paper we follow and extend the work of Hughes and Mallet to construct several non-oscillatory shock-capturing Petrov–Galerkin finite element schemes for solving the one-dimensional Euler equations of gas dynamics. We propose a special weighting function which is different from that in Reference 18. A modified eigenvalue which is a function of ratios of consecutive gradients of conservative variables and the physical eigenvalues is embedded in the weighting function. The mechanism of TVD, TVB and ENO properties can be implemented into the weighting functions in a rather straightforward manner. A linear shape function together with Roe average[20] are used to calculate the integrations of the generalized convection matrix. A one-pass explicit time integration algorithm is employed.

In the following we first review some theoretical aspects of the Euler equations and related concepts employed in this study. A uniformly second-order non-oscillatory scheme using reconstruction via deconvolution of degree two due to Harten *et al.* is briefly described. Forms suitable for extension to the finite element method are given. A Petrov–Galerkin finite element approximation for solving the one-dimensional Euler equations is described. Two different approaches are introduced. The first approach is based on the original Euler equations with a special weighting function which includes a modified eigenvalue to carry the TVD, TVB or ENO mechanism. The second approach is based on Harten's modified flux and a weighting function which is similar to that in Reference 19. A simple explicit time integration method with a lumped mass matrix is adopted.

Numerical experiments are carried out using the present non-oscillatory finite element schemes for the Burgers' equation and the Euler equations. The one-dimensional shock tube problem and the two-blast-wave interaction problem are simulated. A comparison of the performance of each method is made in terms of accuracy and CPU time and some concluding remarks are given.

THEORETICAL CONSIDERATIONS

We consider the motion of a perfect gas in a domain $\Omega \subset R^1$ over a time interval $[0, T]$. Let D denote the space–time domain $D = \Omega \times (0, T)$ and let Γ denote the boundary of Ω. The governing equations of the 1D unsteady inviscid compressible gas dynamics in conservation law form is

$$U_{,t} + F(U)_{,x} = 0 \quad \text{on } \Omega, \tag{1}$$

where a comma stands for differentiation (i.e. $U_{,t} = \partial U/\partial t$). We seek the solution U of equation (1) that satisfies the initial condition

$$U(x, 0) = U_0(x), \quad x \in \Omega \tag{2}$$

and a Dirichlet-type boundary condition

$$\partial U = \mathscr{G} \quad \text{on } \Gamma_{\mathscr{G}}, \tag{3}$$

where U_0 is a given function, ∂ is a boundary operator, $\mathscr{G}$ is a prescribed function and $\Gamma_{\mathscr{G}}$ is a subset of Γ.

In equation (1), $U = [\rho, \rho u, e]^{\mathrm{T}}$ and $F = [\rho u, \rho u^2 + p, u(e+p)]^{\mathrm{T}}$, where ρ is the fluid density, u is the fluid velocity, e is the total energy and p is the pressure. For a perfect gas $p = (\gamma - 1)(e - \rho u^2/2)$, where γ is the ratio of specific heats. Equation (1) can be expressed in quasi-linear form as

$$U_{,t} + A(U)U_{,x} = 0, \qquad A(\mathrm{U}) = \partial F/\partial U, \tag{4}$$

where $A(U)$ is the Jacobian matrix. Owing to the hyperbolicity property of equation (1), A has real eigenvalues

$$a^1 = u, \qquad a^2 = u + c, \qquad a^3 = u - c, \tag{5}$$

where $c = \sqrt{(\gamma p/\rho)}$ is the speed of sound. The corresponding right-eigenvectors are

$$r_1(U) = [1, u, u^2/2]^{\mathrm{T}}, \qquad r_2(U) = [1, u+c, H+uc]^{\mathrm{T}}, \qquad r_3(U) = [1, u-c, H-uc]^{\mathrm{T}}, \tag{6}$$

where $H = (e+p)/\rho = c^2/(\gamma - 1) + \frac{1}{2}u^2$ is the total enthalpy per unit mass. We first form the matrix R, the columns of which are right-eigenvectors r_k,

$$R(U) = [r_1(U), r_2(U), r_3(U)],$$

and then define $l_k(U)$ to be the kth row in R^{-1}, the inverse of $R(U)$. We have

$$\begin{aligned} l_1(U) &= [1 - \Upsilon u^2/2,\ \Upsilon u,\ -\Upsilon], \\ l_2(U) &= [(\Upsilon u^2/2 - u/c)/2,\ (-\Upsilon u + 1/c)/2,\ \Upsilon/2], \\ l_3(U) &= [(\Upsilon u^2/2 + u/c)/2,\ (-\Upsilon u - 1/c)/2,\ \Upsilon/2], \end{aligned} \tag{7}$$

with $\Upsilon = (\gamma - 1)/c^2$. It then follows that

$$A = R \Lambda R^{-1}, \qquad \Lambda = \mathrm{diag}\{a^k\}, \tag{8}$$

and equation (4) can be cast into the following characteristic form:

$$R^{-1}U_{,t}+\Lambda R^{-1}U_{,x}=0. \tag{9}$$

For the purpose of analysis we assume that the coefficient matrix A is 'frozen', i.e. constant. We now define a characteristic variable $V=(v^1, v^2, v^3)^{\mathrm{T}}=R^{-1}U$ and transform equation (8) into the uncoupled system

$$v^k_{,t}+a^k v^k_{,x}=0, \qquad k=1,2,3. \tag{10}$$

Many numerical methods for solving the system (1) can be best understood by looking at the corresponding scheme for (10), i.e. the scalar wave equation (dropping the superscript k)

$$v_{,t}+av_{,x}=0, \qquad a=\text{constant}. \tag{11}$$

NUMERICAL ADVECTION AND NON-OSCILLATORY SCHEMES

Before we turn to the finite element method for solving equation (1), let us first examine a uniformly second-order ENO scheme for equation (11) using the reconstruction via deconvolution (RD) with $N=2$ developed by Harten *et al.*[14–16] Then we examine a second-order TVB scheme due to Shu.[18]

Let us assume that our model consists of n_{el} elements and let e be the variable index for the elements; thus $1\le e\le n_{\mathrm{el}}$ and $\Omega^e=[x_{j-1}, x_j]$, the domain of the eth element, is taken to be an open set and its boundary is denoted by $\overline{\Omega^e}$. For finite difference methods we use the node values while for finite element methods we use both elements and nodes. We further assume uniform discretization ($h^e=h=\Delta x$). Let v_j^n denote the computed approximation to the exact solution $v(x=j\Delta x, t=t^n)$.

Uniformly second-order non-oscillatory schemes

We consider the Harten–Osher non-oscillatory MUSCL-type scheme which uses the reconstruction via deconvolution (RD) approach of degree two for equation (11) with $a>0$.

That is, for $N=2$ using RD one has, for $x_j\le x<x_{j+1}$,

$$Q^2(x;v)=v_j+\frac{x-x_j}{h}\Delta_+v_j+\frac{(x-x_j)(x-x_{j+1})}{2h^2}\bar{m}(\Delta_-\Delta_+v_j, \Delta_+\Delta_+v_j), \tag{12}$$

where $Q(x;v)$ is an ENO piecewise polynomial of order two.

A simple calculation gives the algorithm for $|\sigma|<1$:

$$\begin{aligned} v_j^{n+1}={}&v_j^n-\sigma\Delta_-v_j^n-\sigma\left(\frac{1-\sigma}{2}\right)\Delta_-\{m[\Delta_-v_j^n+\beta\bar{m}(\Delta_-\Delta_+v_j^n, \Delta_-\Delta_-v_j^n),\\ &\Delta_+v_j^n-\beta\bar{m}(\Delta_+\Delta_+v_j^n, \Delta_-\Delta_+v_j^n)]\}. \end{aligned} \tag{13}$$

Here the minmod function m and the function $\bar{m}$ are defined respectively by

$$m(a,b)=\begin{cases}\operatorname{sgn}(a)\min(|a|,|b|), & \text{if } ab\ge 0,\\ 0 & \text{if } ab<0,\end{cases} \tag{14}$$

$$\bar{m}(a,b)=\begin{cases}a & \text{if } |a|\le|b|,\\ b & \text{if } |a|>|b|.\end{cases} \tag{15}$$

For the purpose of the present finite element methods, equation (13) can be cast into the following form:

$$v_j^{n+1} = v_j^n - \sigma\Delta_- v_j^n - \sigma\left(\frac{1-\sigma}{2}\right)\Delta_-\{m[1+\beta\bar{m}(r^+-1,\ 1-r^-),\ r^+-\beta\bar{m}(r^{++}-r^+, r^+-1)]\Delta_- v_j^n\}, \tag{16}$$

where the consecutive gradients r^+, r^{++}, r^- and r^{--} at $j-\frac{1}{2}$ are given by

$$\begin{aligned} r_{j-1/2}^+ &= \Delta_+ v_j/\Delta_- v_j, & r_{j-1/2}^{++} &= \Delta_+ v_{j+1}/\Delta_- v_j, \\ r_{j-1/2}^- &= \Delta_- v_{j-1}/\Delta_- v_j, & r_{j-1/2}^{--} &= \Delta_- v_{j-2}/\Delta_- v_j, \end{aligned} \tag{17}$$

and $\Delta_\pm$ are the usual difference operators $\Delta_\pm v_j = \pm(v_{j\pm1} - v_j)$.

Here $\lambda = \Delta t/\Delta x$ is the mesh ratio and $\sigma = \lambda a$ is the Courant number, which can be a variable. The scheme defined by equation (13) is stable for $|\sigma| \le 1$.

For $\beta = 0$ we recover the second-order TVD scheme of Harten.[8]

For $\beta = \frac{1}{2}$ we have the uniformly second-order ENO scheme of Harten and Osher.[14]

In equation (13) one can replace both of the $\bar{m}$ by m to obtain another non-oscillatory scheme.[14] For further details of the methods the reader is encouraged to read the original papers.[14–16]

It is also noted that other forms of equation (13) can be used to construct different algorithms, such as the following:

$$\begin{aligned} v_j^{n+1} = v_j^n - \sigma\Delta_- v_j^n - \Delta_-\Bigg\{ m\Bigg[&\sigma\left(\frac{1-\sigma}{2}\right)\Delta_- v_j^n + \beta\bar{m}\left(\Delta_-\sigma\left(\frac{1-\sigma}{2}\right)\Delta_- v_j^n,\ \Delta_+\sigma\left(\frac{1-\sigma}{2}\right)\Delta_- v_j^n\right), \\ &\sigma\left(\frac{1-\sigma}{2}\right)\Delta_+ v_j^n - \beta\bar{m}\left(\Delta_-\sigma\left(\frac{1-\sigma}{2}\right)\Delta_+ v_j^n,\ \Delta_+\sigma\left(\frac{1-\sigma}{2}\right)\Delta_+ v_j^n\right)\Bigg]\Bigg\}, \end{aligned} \tag{18}$$

$$\begin{aligned} v_j^{n+1} = v_j^n - \lambda\Delta_- f_j^n - \lambda\Delta_-\Bigg\{ m\Bigg[&\left(\frac{1-\sigma}{2}\right)\Delta_- f_j^n + \beta\bar{m}\left(\Delta_-\left(\frac{1-\sigma}{2}\right)\Delta_- f_j^n,\ \Delta_+\left(\frac{1-\sigma}{2}\right)\Delta_- f_j^n\right), \\ &\left(\frac{1-\sigma}{2}\right)\Delta_+ f_j^n - \beta\bar{m}\left(\Delta_-\left(\frac{1-\sigma}{2}\right)\Delta_+ f_j^n,\ \Delta_+\left(\frac{1-\sigma}{2}\right)\Delta_+ f_j^n\right)\Bigg]\Bigg\}. \end{aligned} \tag{19}$$

Comparing equations (18) and (19) with equation (13), it is noted that we have used in (18) and (19) quantities of the form

$$\sigma\left(\frac{1-\sigma}{2}\right)\Delta_- v_j \quad \text{and} \quad \operatorname{sgn} a\left(\frac{1-\sigma}{2}\right)\Delta_- f_j$$

respectively as the building elements, and the limiting functions m and $\bar{m}$ are limiting on such quantities. In Reference 17 equation (19) has been employed to construct uniformly second-order non-oscillatory schemes for the two-dimensional Euler equations in general curvilinear co-ordinates.

It is rather constructive to have the schemes written in this form, since one can easily extend the algorithm for a single wave equation to that for a scalar conservation law and then to hyperbolic systems of conservation laws in a straightforward manner.

Total variation bounded scheme

In Reference 18 a TVB modification of Harten's second-order TVD scheme for conservation laws was given. Applying the TVB modification procedure to equation (13) with $\beta = 0$, we have

$$v_j^{n+1} = v_j^n - \sigma\Delta_- v_j^n - \sigma\left(\frac{1-\sigma}{2}\right)\Delta_- \{\tfrac{1}{2}[mc(M, \Delta x)(\Delta_- v_j^n, b\Delta_+ v_j^n) + mc(M, \Delta x)(\Delta_+ v_j^n, b\Delta_- v_j^n)]\}, \tag{20}$$

where

$$mc(M, \Delta x)(\Delta_+ v_j^n, b\Delta_- v_j^n) = m[\Delta_+ v_j^n, b\Delta_- v_j^n + M\Delta x^2 \operatorname{sgn}(\Delta_+ v_j^n)], \tag{21}$$

with $1 < b \leq 3$ and $50 \leq M \leq 200$. The scheme defined by equation (20) is TVB and second-order accurate except at sonic points under the CFL condition

$$\lambda \max_j |a_j^l| \leq \frac{4}{b+1} - 1. \tag{22}$$

We can express equation (20) in the form

$$v_j^{n+1} = v_j^n - \sigma\Delta_- v_j^n - \sigma\left(\frac{1-\sigma}{2}\right)\Delta_- \{\tfrac{1}{2}[\overline{mc}(M, \Delta x)(1, br^+) + \overline{mc}(M, \Delta x)(r^+, b)]\Delta_- v_j^n\}, \tag{23}$$

where $\overline{mc}(M, \Delta x)$ is defined as

$$\overline{mc}(M, \Delta x)(1, br^+)\Delta_- v_j^n = m\left(1, br^+ + \frac{M\Delta x^2}{\Delta_- v_j}\operatorname{sgn}(\Delta_- v_j)\right)\Delta_- v_j, \tag{24a}$$

$$\overline{mc}(M, \Delta x)(r^+, b)\Delta_- v_j = m\left(r^+, b + \frac{M\Delta x^2}{\Delta_- v_j}\operatorname{sgn}(\Delta_+ v_j)\right)\Delta_- v_j^n. \tag{24b}$$

PETROV–GALERKIN FINITE ELEMENT FORMULATION

In this section we follow closely the work of Hughes and Mallet[19] except for a different definition of the weighting function and consider a weighted residual formulation for the problem defined by equations (1)–(3).

We assume that trial functions U satisfy $\partial U = \mathscr{G}$ on $\Gamma_{\mathscr{G}}$ and the weighting functions W satisfy $\partial W = 0$ on $\Gamma_{\mathscr{G}}$. Thus all Dirichlet-type boundary conditions are treated as essential boundary conditions in the present work. The trial function U and the weighting function W are assumed to be taken from the same class of typical C^0 finite element interpolations.

By applying the Petrov–Galerkin finite element method to equations (1)–(3) we have the following:

$$0 = \sum_{e=1}^{n_{el}} \int_{\Omega_e} W^t(U_{,t} + F_{,x})\mathrm{d}\Omega. \tag{25}$$

We expand U in terms of a set of finite element basis, or shape functions as follows:

$$U(x, t) = \sum_j N_j(x)U_j(t), \tag{26}$$

where j is a nodal index, N_j is the usual linear hat function associated with node j, and U_j is the value of U at node j.

We also approximate the flux vector F in the following form:

$$F(x, t) = \sum_j N_j(x) F_j(t). \tag{27}$$

Spatial discretization of the weighted residual equation (25) via finite elements leads to the following semidiscrete system of ordinary differential equations:

$$M\dot{v} + Cv = 0, \tag{28}$$

where $M = M(v, t)$ is the generalized mass matrix, $C = C(v, t)$ is the generalized convection matrix, v is the vector of nodal values of U and a superposed dot denotes time differentiation.

The arrays in equation (28) are assembled from element contributions:

$$M = \mathscr{A}_{e=1}^{n_{el}}(m^e), \tag{29}$$

$$m^e = [m_{jk}^e], \tag{30}$$

$$m_{jk}^e = \int_{\Omega^e} \tilde{N}_j N_k \, d\Omega, \tag{31}$$

$$C = \mathscr{A}_{e=1}^{n_{el}}(c^e), \tag{32}$$

$$c^e = [c_{jk}^e], \tag{33}$$

$$c_{jk}^e = \int_{\Omega^e} \tilde{N}_j A N_{k,x} \, d\Omega, \tag{34}$$

where the symbol $\mathscr{A}$ represents the finite element assembly operator, j and k are local element node numbers and $\tilde{N}_j$ is the weighting function matrix.

In Reference 19 Hughes and Mallet considered a one-parameter family of weighting functions of the following form:

$$\tilde{N}_j^l = \tfrac{1}{2}[\chi_j I + R\tilde{l}\,\mathrm{sgn}(N_{j,x}\Lambda)R^{-1}], \tag{35}$$

where I is the identity matrix and χ_j is the characteristic function associated with node j. That is,

$$\chi_j = \begin{cases} 1, & x \in [x_{j-1}, x_{j+1}], \\ 0, & \text{otherwise}, \end{cases} \tag{36}$$

and, in the element subdomain $[x_j, x_{j+1}]$,

$$\tilde{l} = \mathrm{diag}(l^1, l^2, l^3), \tag{37}$$

where l^i are limiters which are limiting on the characteristic variables $\alpha_j = R^{-1}U_j$. For $\tilde{l} = I$ one recovers Osher's method. For further details see Reference 19.

In the present work the weighting function matrix $\tilde{N}$ is given by

$$\tilde{N}_j = \tfrac{1}{2}[\chi_j I + R\,\mathrm{diag}\{(\tilde{a}^l/a^l)N_{j,x}\}R^{-1}]. \tag{38}$$

It is noted that all the limiters are absorbed in $\tilde{a}^l$ and the difference between equation (35) and equation (38) lies in the quantities which were limited. They are identical only for the scalar case, i.e. the scalar wave equation.

We use standard C^0 piecewise linear interpolation for the shape function and adopt Roe's average to approximate the integration in equation (35). Then we have

$$c_{jk}^e = \begin{bmatrix} -\tilde{A}^- & \tilde{A}^- \\ -\tilde{A}^+ & \tilde{A}^+ \end{bmatrix}, \tag{39}$$

where

$$\tilde{A}^{\pm} = R\,\mathrm{diag}\{\tilde{a}^{l\pm}\}R^{-1}, \qquad \tilde{a}^{l\pm} = (a^l \pm \tilde{a}^l)/2. \tag{40}$$

In equation (40) the a^l are given by equation (5) and the $\tilde{a}^l$ are the averaged modified eigenvalues in the element subdomain $[x_j, x_{j+1}]$ which are defined in such a way as to make the resulting scheme capable of precise resolution of discontinuities while maintaining formal accuracy in the smooth region. The main objective of the present work is to incorporate the non-oscillatory mechanisms of TVD, TVB and ENO in these modified eigenvalues $\tilde{a}^l$.

The transient algorithm for the present method is the one-step explicit scheme defined as

$$a = -\bar{M}^{-1}C(v^n)v^n, \tag{41}$$

$$v^{n+1} = v^n + \Delta t a. \tag{42}$$

In the above, $\tilde{M}$ is a lumped mass matrix which is given by

$$\bar{M}_{jk} = \begin{cases} \frac{1}{2}(\Delta x_{j-1/2} + \Delta x_{j+1/2})I & \text{if } k=j \\ 0 & \text{otherwise.} \end{cases} \tag{43}$$

In the following we consider TVD, TVB and ENO schemes. We also consider a symmetric TVD scheme[26] which is a generalization of Roe's[27] and Davis's[28] TVD Lax–Wendroff scheme. The definition of $\tilde{a}^l$ at $j+\frac{1}{2}$ for each method is listed below.

Second-order symmetric TVD scheme (Roe–Davis–Yee[27, 28, 26])

$$(\tilde{a}^l_{j+1/2})^{\mathrm{SYM}} = \Psi(a^l_{j+1/2}) - 2\zeta(a^l_{j+1/2})(Q^{l+} + Q^{l-} - 1)_{j+1/2}. \tag{44}$$

Second-order TVD scheme (Harten[8])

$$(\tilde{a}^l_{j+1/2})^{\mathrm{TVD}} = \Psi(a^l_{j+1/2} + \gamma^l_{j+1/2}) - \zeta(a^l_{j+1/2})(Q^{l+} + Q^{l-})_{j+1/2}. \tag{45}$$

Second-order TVB scheme (Shu[18])

$$(\tilde{a}^l_{j+1/2})^{\mathrm{TVB}} = \Psi(a^l_{j+1/2} + \tilde{\gamma}^l_{j+1/2}) - \zeta(a^l_{j+1/2})(\tilde{Q}^{l+} + \tilde{Q}^{l-})_{j+1/2}. \tag{46}$$

Uniformly second-order ENO scheme (Harten–Osher[14])

$$(\tilde{a}^l_{j+1/2})^{\mathrm{ENO2}} = \Psi(a^l_{j+1/2} + \hat{\gamma}^l_{j+1/2}) - \zeta(a^l_{j+1/2})(\hat{Q}^{l+} + \hat{Q}^{l-})_{j+1/2}. \tag{47}$$

In the above the limiter functions $Q^{l\pm}$, $\tilde{Q}^{l\pm}$ and $\hat{Q}^{l\pm}$ are given respectively by

$$Q^{l\pm}_{j+1/2} = \max[0, \min(Cr^{\pm}, 1), \min(r^{\pm}, C)], \quad 1 \le C \le 2 \quad \begin{cases} C = 1, & \text{Harten,} \\ C = 2, & \text{Roe's superbee,} \\ 1 < C < 2, & \text{Sweby,} \end{cases} \tag{48}$$

$$\tilde{Q}^{l+}_{j+1/2} = 0{\cdot}5[\overline{mc}(r^+, b) + \overline{mc}(1, br^+)] \tag{49a}$$

$$\tilde{Q}^{l-}_{j+1/2} = 0{\cdot}5[\overline{mc}(1, br^-) + \overline{mc}(r^-, b)], \tag{49b}$$

$$\hat{Q}^{l+}_{j+1/2} = m[r^+ - \beta\bar{m}(r^{++} - r^+, r^+ - 1), 1 + \beta\bar{m}(r^+ - 1, 1 - r^-)], \tag{50a}$$

$$\hat{Q}^{l-}_{j+1/2} = m[1 - \beta\bar{m}(r^+ - 1, 1 - r^-), r^- + \beta\bar{m}(1 - r^-, r^- - r^{--})]. \tag{50b}$$

The functions γ^l, $\tilde{\gamma}^l$ and $\hat{\gamma}^l$ are given by

$$\gamma^l_{j+1/2} = \begin{cases} \zeta(a^l_{j+1/2})(Q^{l+} - Q^{l-})_{j+1/2} & \text{if } \Delta_+ u^l_j \neq 0, \\ 0 & \text{otherwise,} \end{cases} \tag{51}$$

$$\tilde{\gamma}^l_{j+1/2} = \begin{cases} \zeta(a^l_{j+1/2})(\tilde{Q}^{l+} - \tilde{Q}^{l-})_{j+1/2} & \text{if } \Delta_+ u^l_j \neq 0, \\ 0 & \text{otherwise,} \end{cases} \tag{52}$$

$$\hat{\gamma}^l_{j+1/2} = \begin{cases} \zeta(a^l_{j+1/2})(\hat{Q}^{l+} - \hat{Q}^{l-})_{j+1/2} & \text{if } \Delta_+ u^l_j \neq 0, \\ 0 & \text{otherwise,} \end{cases} \tag{53}$$

and

$$\zeta(z) = \tfrac{1}{2}[\Psi(z) - \lambda z^2], \tag{54}$$

$$\Psi(z) = \begin{cases} |z| & \text{if } |z| \geq \varepsilon, \\ (z^2+\varepsilon^2)/2\varepsilon & \text{if } |z| < \varepsilon. \end{cases} \tag{55}$$

Here ε is a small positive constant. The gradient ratios r^+, r^-, r^{++} and r^{--} are evaluated at $j+\frac{1}{2}$. The u^l_j are components of the conservative variables U_j.

For the system cases the definitions of r^+, r^-, r^{++} and r^{--} in equation (17) are given in terms of the characteristic variables $\alpha_{j+1/2} = R^{-1}_{j+1/2}(U_{j+1} - U_j)$ and R^{-1} is evaluated using the Roe average. They are

$$r^{l+}_{j-1/2} = \alpha^l_{j+1/2}/\alpha^l_{j-1/2}, \qquad r^{l++}_{j-1/2} = \alpha^l_{j+3/2}/\alpha^l_{j-1/2},$$
$$r^{l-}_{j-1/2} = \alpha^l_{j-3/2}/\alpha^l_{j-1/2}, \qquad r^{l--}_{j-1/2} = \alpha^l_{j-5/2}/\alpha^l_{j-1/2}.$$

In equation (47) if we set $\beta = 0$ we recover equation (45) with $C = 1$. The selection of the parameter C used in equation (48) was discussed by Sweby.[9]

It is noted that if one takes $\tilde{a}^l = \Psi(a^l)$ in equation (38) then one has a first-order upwind finite element scheme (e.g. Osher's method).

For the scalar wave equation and uniform elements one can deduce that the second-order ENO scheme is identical to the uniformly second-order ENO scheme in Reference 14 constructed using reconstruction via deconvolution (RD) with $N = 2$.

We shall denote the schemes defined by equations (44)–(47) as the SYM, TVD, TVB and ENO2 schemes respectively.

MODIFIED FLUX APPROACH

Another way to achieve higher-order accuracy is based on an approach similar to Harten's modified flux approach. Let us consider a scalar conservation law

$$u_{,t} + f(u)_{,x} = 0, \qquad a = \partial f/\partial u, \tag{56}$$

with weighting function defined as

$$\tilde{N}_j = \tfrac{1}{2}[\chi_j + \operatorname{sgn}(aN_{j,x})]. \tag{57}$$

The resulting scheme is first-order accurate. Consider a modified version (56),

$$u_{,t} + (f+g)_{,x} = 0, \tag{58}$$

with weighting function

$$\tilde{N}_j = \tfrac{1}{2}[\chi_j + \operatorname{sgn}(a^M N_{j,x})], \tag{59}$$

where

$$a^M = a + \bar{\gamma}.$$

Here $\bar{\gamma}$ is the characteristic speed introduced by the additional flux function g. The value of g at node j is defined by

$$g_j = S\max(0, \min(\zeta_{j+1/2}|\Delta_+ u_j|, S\zeta_{j-1/2}\Delta_- u_j)], \tag{60}$$

where

$$S = \operatorname{sgn}(\Delta_+ u_j), \tag{61}$$

$$\bar{\gamma} = \begin{cases} (g_{j+1} - g_j)/\Delta_+ u_j & \text{if } \Delta_+ u_j \neq 0, \\ 0 & \text{otherwise.} \end{cases} \tag{62}$$

The functions $\zeta(z)$ and $\Psi(z)$ are the same as those given before.

The convection matrix for the jth element is

$$c^e_{jk} = \begin{bmatrix} -a^{M-} & a^{M-} \\ -a^{M+} & a^{M+} \end{bmatrix}, \tag{63}$$

where

$$a^{M\pm} = (a^M \pm |a^M|)/2. \tag{64}$$

For the various schemes we can simply give a proper definition of a^M as in the previous section. This formulation can also be extended to non-linear systems. However, this formulation is not as flexible as those mentioned above.

NUMERICAL RESULTS

The inviscid Burgers' equation

In the first example we show the results of applying the various schemes to the inviscid Burgers' equation

$$u_{,t} + (u^2/2)_{,x} = 0, \tag{65a}$$

$$u(x, 0) = \tfrac{1}{4} + \tfrac{1}{2}\sin(\pi x), \quad -1 \leq x \leq 1. \tag{65b}$$

The exact solution is smooth up to $t = 2/\pi$, then it develops a moving shock which interacts with the rarefaction waves. We get the exact solution by using Newton–Raphson iteration. In this example we replace the weighting function in (38) by

$$\tilde{N}_j = \tfrac{1}{2}[\chi_j + (\tilde{a}/a^l)N_{j,x}], \tag{66}$$

with $a^l = u$.

Tables I–IV list the L_∞-error, L_1-error and L_2-error of the numerical solution of equation (65) using the SYM, TVD, TVB and ENO2 schemes respectively for a mesh refinement sequence $n_{el} = 20$, 40 and 80. The output time is $t = 0{\cdot}3$ when the solution is still smooth and CFL $= 0{\cdot}5$ was used for each calculation. For the TVB results, $b = 2$ and $M = 50$ were used. The value of r in Tables I–IV is the computed order of accuracy. From Tables III and IV we find that the computational order of accuracy of the TVB and ENO2 schemes is similar. Comparing the

Table I. Errors in the numerical solution of equation (65) at $t = 0{\cdot}3$; SYM scheme

N	L_1	r	L_2	r	L_∞	r
20	1·643 (−2)		1·327 (−2)		2·159 (−2)	
40	4·419 (−3)	1·89	4·264 (−3)	1·64	9·300 (−3)	1·22
80	1·221 (−3)	1·85	1·392 (−3)	1·62	4·096 (−3)	1·18

Table II. Errors in the numerical solution of equation (65) at $t = 0{\cdot}3$; TVD scheme

N	L_1	r	L_2	r	L_∞	r
20	9·772 (−3)		9·147 (−3)		1·538 (−2)	
40	2·715 (−3)	1·85	2·750 (−3)	1·73	6·517 (−3)	1·24
80	7·107 (−4)	1·93	8·661 (−4)	1·67	2·976 (−3)	1·13

Table III. Errors in the numerical solution of equation (65) at $t = 0{\cdot}3$; TVB scheme

N	L_1	r	L_2	r	L_∞	r
20	7·062 (−3)		6·934 (−3)		1·090 (−2)	
40	1·656 (−3)	2·09	1·746 (−3)	1·99	3·333 (−3)	1·71
80	4·080 (−4)	2·02	4·295 (−4)	2·02	8·727 (−4)	1·93

Table IV. Errors in the numerical solution of equation (65) at $t = 0{\cdot}3$; ENO2 scheme

N	L_1	r	L_2	r	L_∞	r
20	6·966 (−3)		6·574 (−3)		1·068 (−2)	
40	1·659 (−3)	2·07	1·707 (−3)	1·95	3·328 (−3)	1·68
80	4·078 (−4)	2·02	4·321 (−4)	1·98	8·739 (−4)	1·93

results in Tables I–IV we find that the computational order r of the SYM and TVD schemes is inferior to that of the TVB and ENO2 schemes. In Figures 1–4 we show the solutions at time $2/\pi$ using the above four schemes with 20, 40 and 80 elements. At this time the shock begins to form and interacts with the rarefaction waves. At time $t = 1{\cdot}1$ the interaction between the shock and the rarefaction waves is over. The solution becomes monotone between the shocks. Figures 5–8 show the solutions at time $t = 1{\cdot}1$ with 20, 40 and 80 elements. We see that there is a very good shock transition in each case and no oscillations are observed.

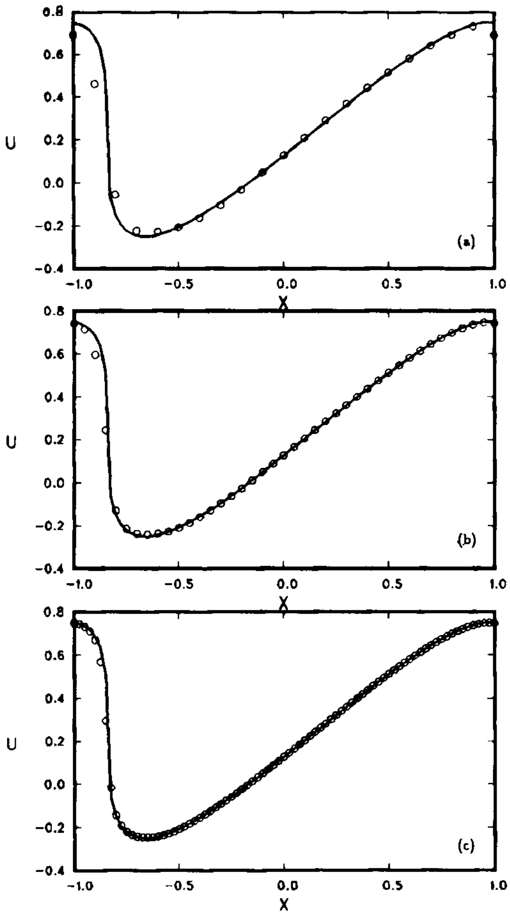

Figure 1. Finite element solution of inviscid Burgers' equation at time $t=2/\pi$ using the SYM scheme: (a) $\Delta x=1/10$; (b) $\Delta x=1/20$; (c) $\Delta x=1/40$

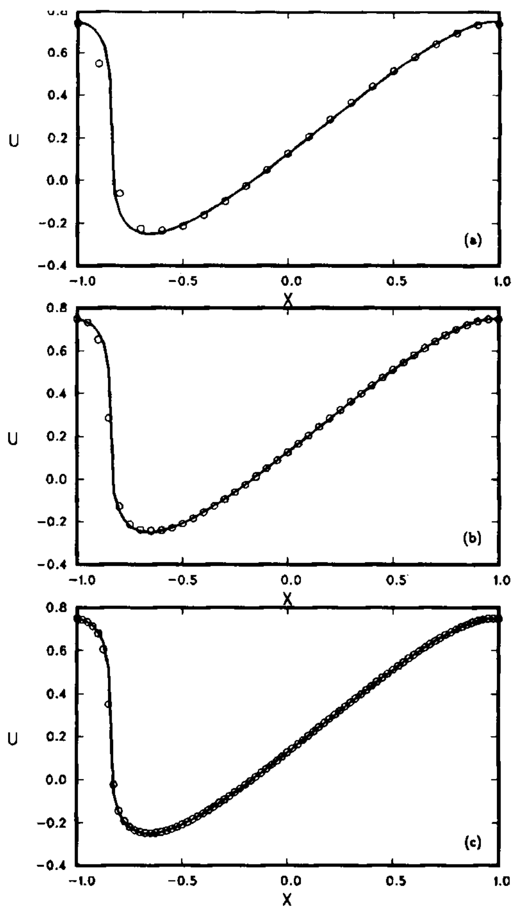

Figure 2. Same as Figure 1 for the TVD scheme

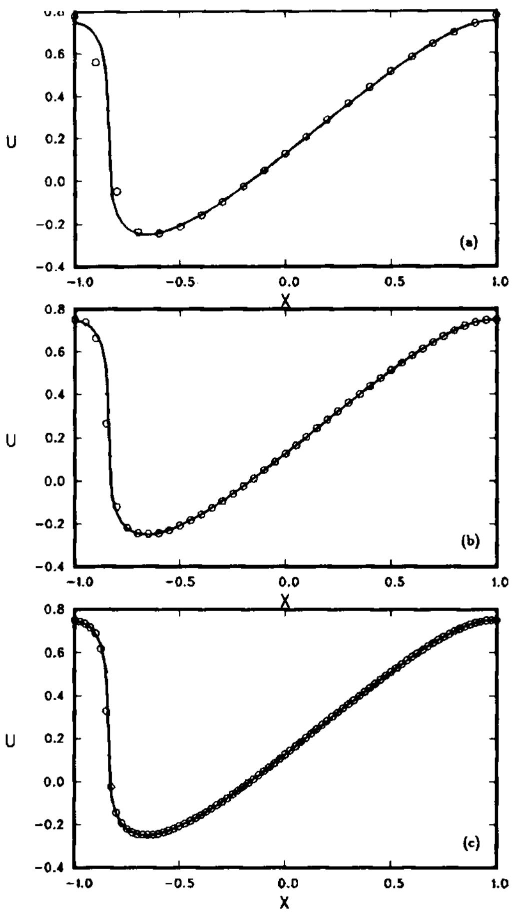

Figure 3. Same as Figure 1 for the TVB scheme

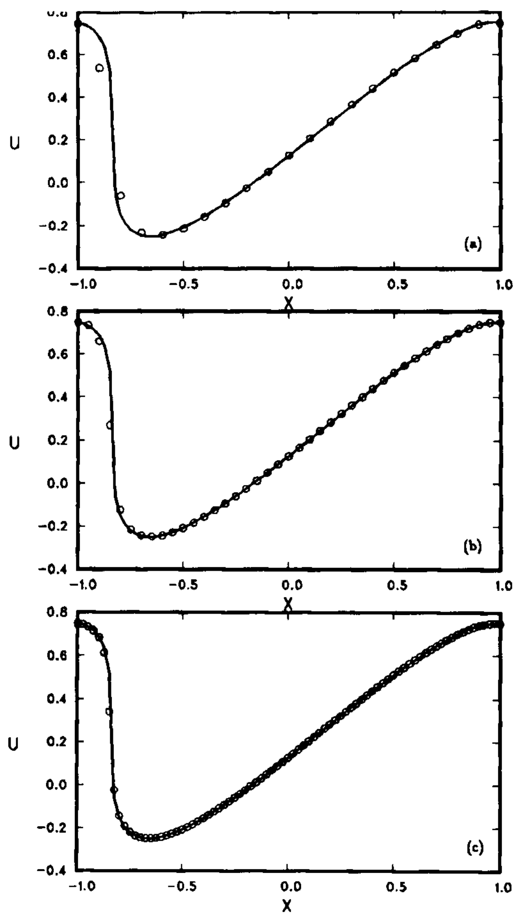

Figure 4. Same as Figure 1 for the ENO2 scheme

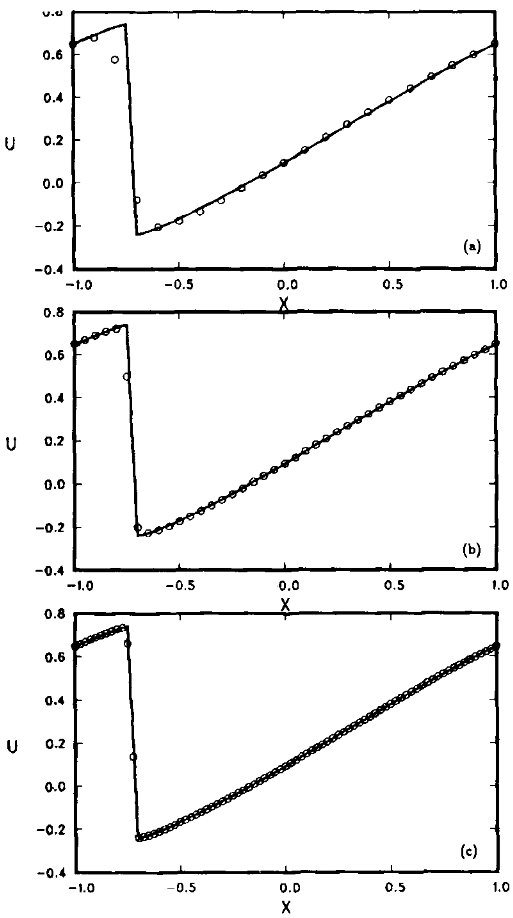

Figure 5. Finite element solution of inviscid Burgers' equation at time $t=1.1$ using the SYM scheme: (a) $\Delta x=1/10$; (b) $\Delta x=1/20$; (c) $\Delta x=1/40$

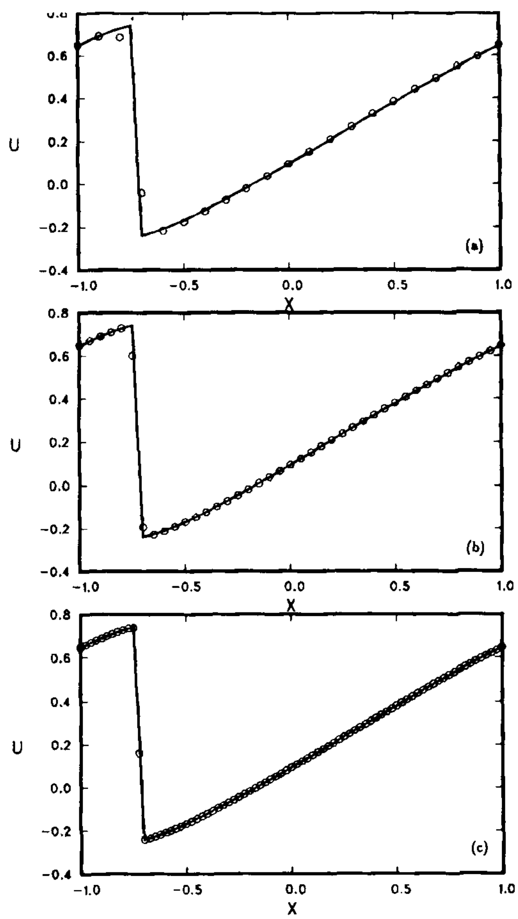

Figure 6. Scheme as Figure 5 for the TVD scheme

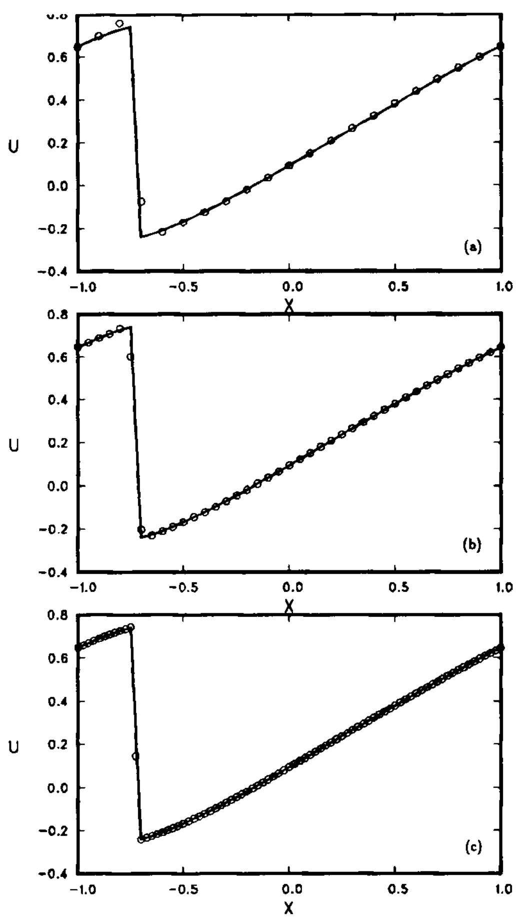

Figure 7. Same as Figure 5 for the TVB scheme

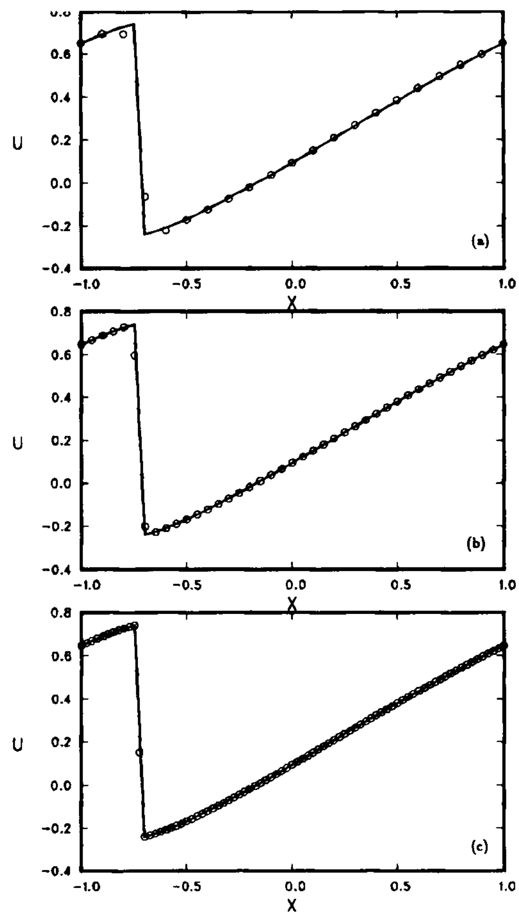

Figure 8. Same as Figure 5 for the ENO2 scheme

The shock tube problem

For the hyperbolic system of conservation laws we consider the one-dimensional Euler equations and simulate the shock tube problem proposed by Sod.[29] The initial conditions at both sides of the diaphragm (initially at $x_0 = 0{\cdot}5$) are

$$\rho_L = 1{\cdot}0, \qquad u_L = 0, \qquad p_L = 1{\cdot}0,$$
$$\rho_R = 0{\cdot}125, \qquad u_R = 0, \qquad p_R = 0{\cdot}1,$$

where the subscripts L and R stand for the left and right side of the diaphragm respectively. The number of elements used is 100. The results at time $t = 0{\cdot}24$ (after 60 integration steps) are shown together with the exact solution (solid line) in Figures 9–12 for each method. From Figure 9 we find that the SYM scheme is more diffusive than the other schemes for the solution near the contact discontinuity. From Figures 10–12, we observe that the TVB and ENO2 schemes demonstrate slight oscillation near the shock but give sharper resolution near the contact discontinuity. These mild oscillatory behaviours are allowable features of the essentially non-oscillatory schemes.

The CPU times needed on a Convex C-1 computer for 60 time integrations using the SYM, TVD, TVB and ENO2 schemes are 3·16, 3·16, 3·46 and 3·35 respectively.

We also experimented with the scheme defined by equation (45) using the different formulation with different weighting function. Since the results were almost the same as those of the TVD scheme, we do not include those figures here.

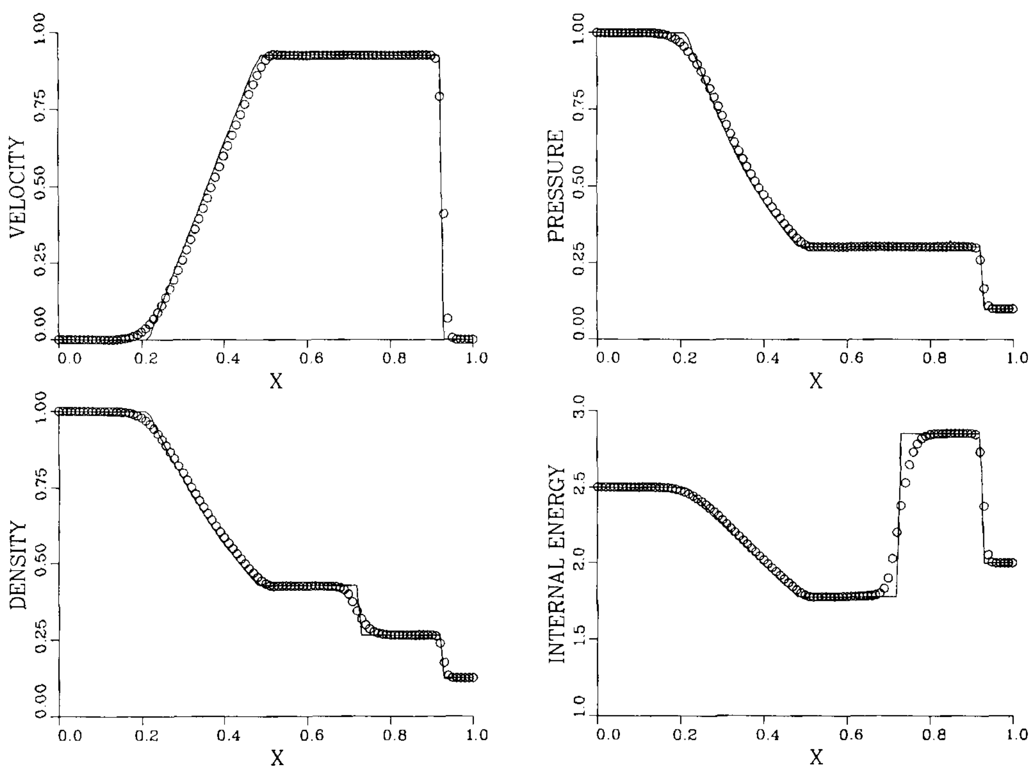

Figure 9. Solution of 1D shock tube flow using the SYM scheme

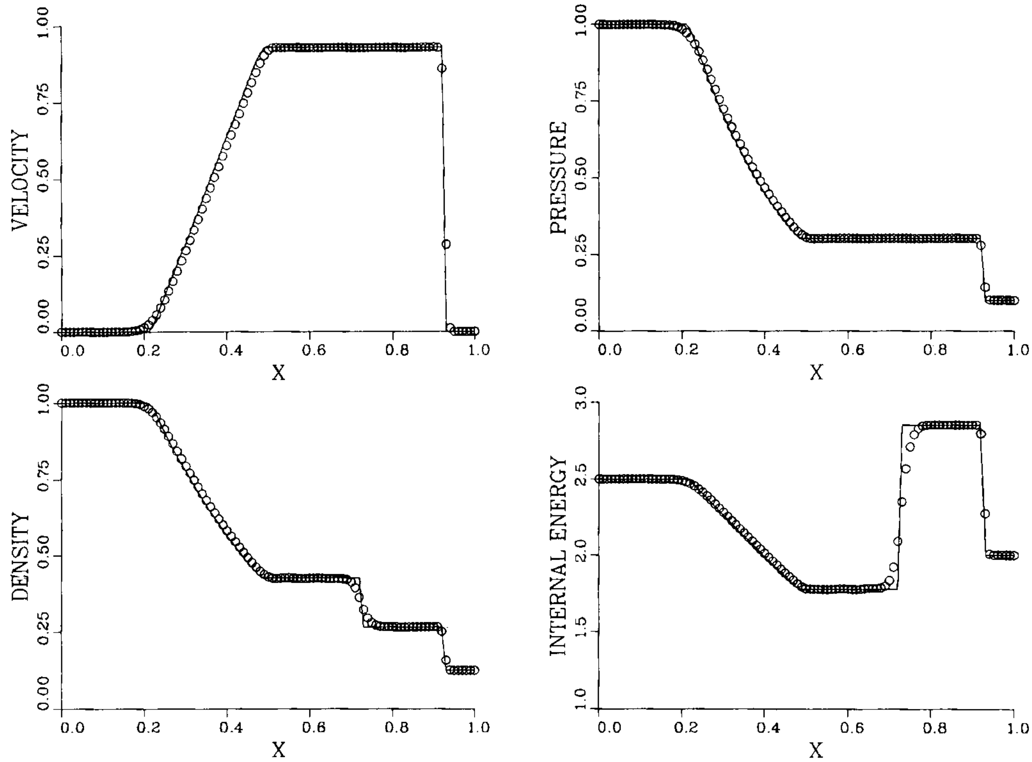

Figure 10. Solution of 1D shock tube flow using the TVD scheme

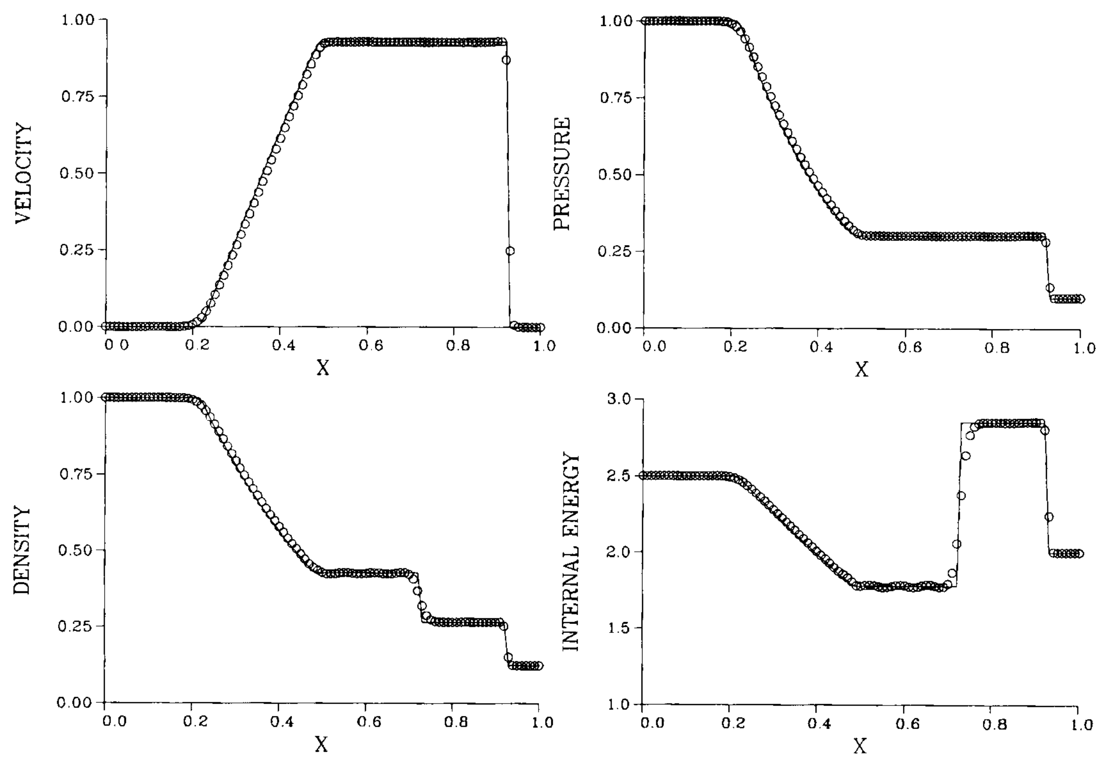

Figure 11. Solution of 1D shock tube flow using the TVB scheme

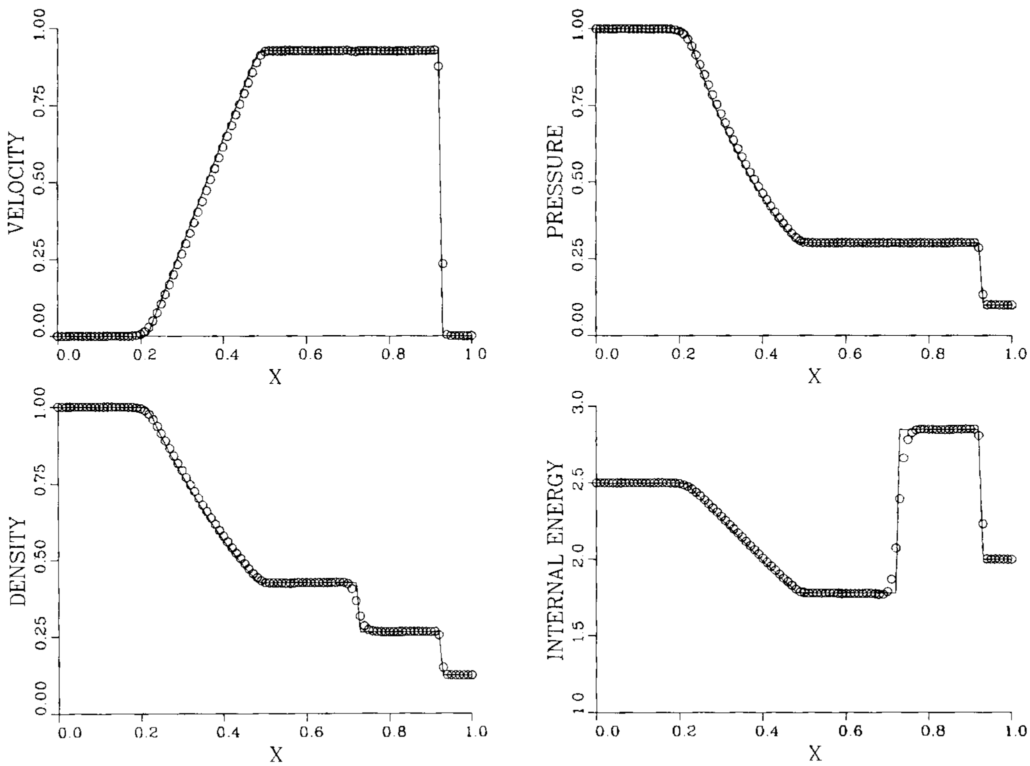

Figure 12. Solution of 1D shock tube flow using the ENO2 scheme

The two-blast-wave interaction problem

The third numerical experiment is the problem of two interacting blast waves suggested by Woodward and Colella; we refer the reader to Reference 30 where a comprehensive comparison of the performance of various schemes for this problem was presented. The initial conditions are given as follows:

$$\rho_L = 1, \quad u_L = 0, \quad p_L = 1000, \quad 0 \le x < 0{\cdot}1,$$
$$\rho_M = 1, \quad u_M = 0, \quad p_M = 0{\cdot}01, \quad 0{\cdot}1 \le x < 0{\cdot}9,$$
$$\rho_R = 1, \quad u_R = 0, \quad p_R = 100, \quad 0{\cdot}9 \le x < 1.$$

The boundaries at $x = 0$ and $x = 1$ are solid walls and reflection boundary conditions are employed. In our calculations we used $\Delta x = 0{\cdot}005$ (200 elements) and CFL = 0·95. Figures 13–16 show the density and velocity distributions for the SYM, TVD, TVB and ENO2 schemes respectively. The solid line is the 'exact' solution taken from Reference 30 using a scanner, while the circles are the present numerical results. The quality of the results for the ENO2 scheme is better than for those of the TVD scheme, as can be seen from the height of the first peak in the density profile. Again, slight oscillations are observed for the TVB and ENO2 schemes. In general, good results are obtained in all cases. The CPU times for this problem using the SYM, TVD, TVB and ENO2 schemes are 38·66, 38·79, 40·09 and 41·55 s respectively. All the calculations were done on a Convex C1 computer.

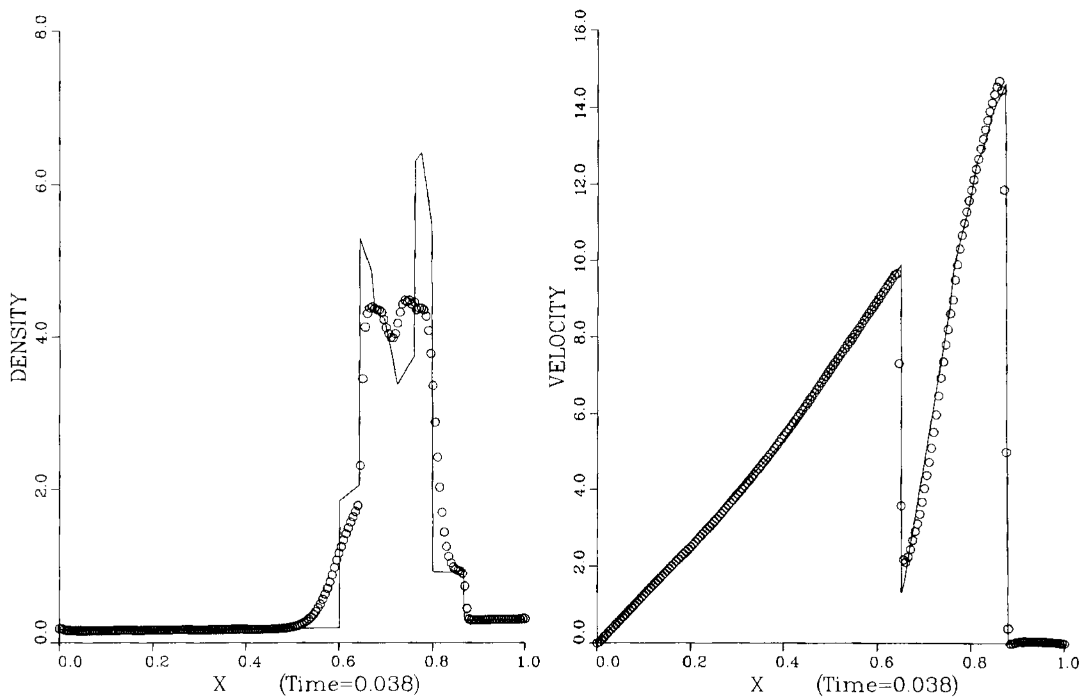

Figure 13. Solution of two interacting blast waves using the SYM scheme

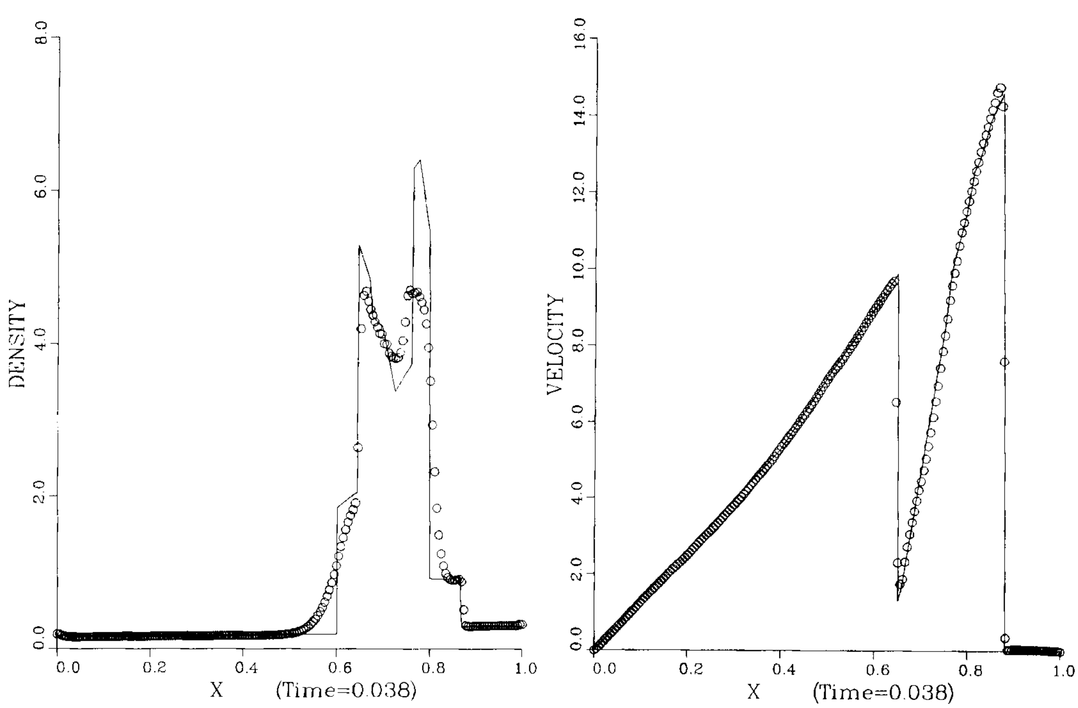

Figure 14. Solution of two interacting blast waves using the TVD scheme

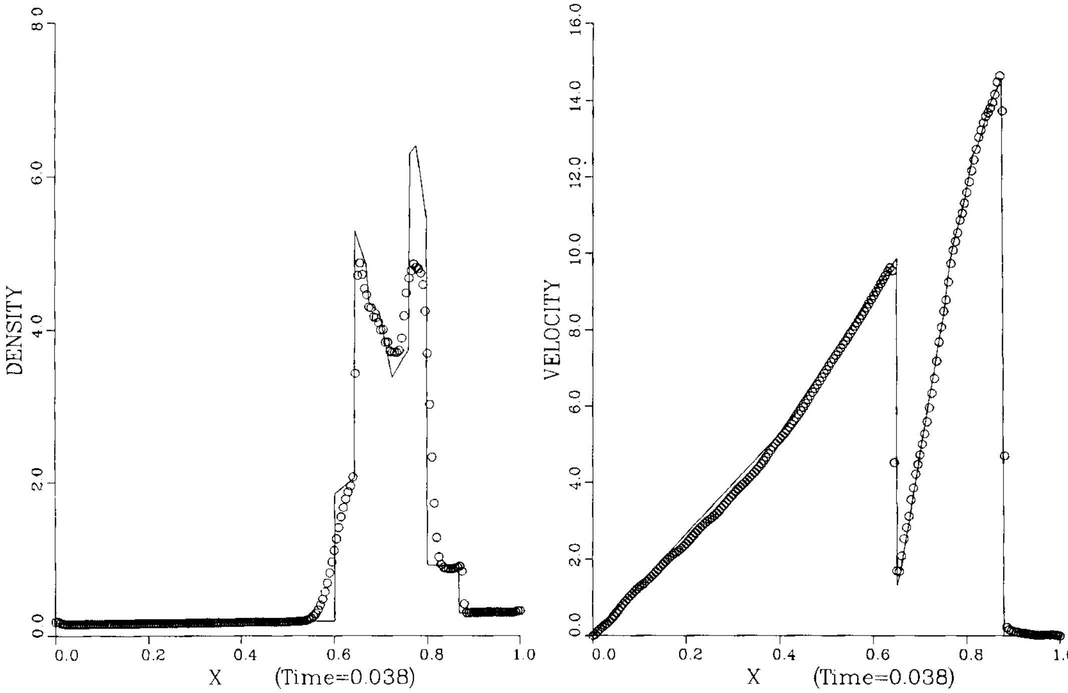

Figure 15. Solution of two interacting blast waves using the TVB scheme

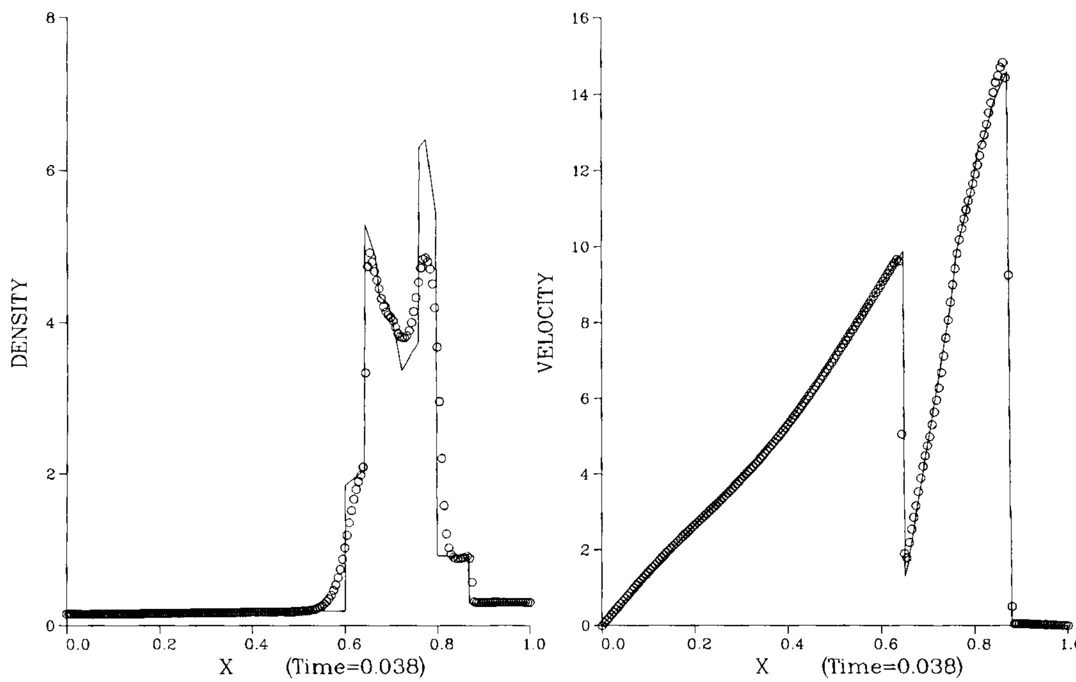

Figure 16. Solution of two interacting blast waves using the ENO2 scheme

CONCLUDING REMARKS

In this paper, following and extending the work of Hughes and Mallet,[19] we have described a new class of non-oscillatory shock-capturing Petrov–Galerkin finite element methods for the one-dimensional compressible Euler equations and applied them to unsteady gas-dynamical problems with strong shocks. Two different approaches are introduced. The first approach is based on introducing a modified eigenvalue into the weighting function which enables us to accommodate various different non-oscillatory mechanisms such as total variation diminishing, total variation bounded and essentially non-oscillatory. The second approach, which is less flexible than the first, is based on a modified flux function with a weighting function similar to that of Hughes and Mallet. A one-pass explicit time integration scheme with a 'lumped' mass matrix was employed for both approaches. The Roe average was used to evaluate the stiff matrix. Numerical experiments with the present finite element methods for the one-dimensional Euler equations indicate that accurate solutions in the smooth region and non-oscillatory solutions at discontinuities are obtainable.

The extension to multidimensional problems is a subject of future work. We refer the reader to Reference 31 for multidimensional advective–diffusive systems.

ACKNOWLEDGEMENTS

The authors would like to thank the reviewers for their valuable comments. This research was done under the auspices of the National Science Council, Republic of China, under Grants NSC 77-0210-D002-03 and 78-0210-D002-11.

REFERENCES

1. L. B. Wahlbin, 'A dissipative Galerkin method applied to some quasi-linear hyperbolic equations', *RAIRO*, **8**, 109–117 (1974).
2. J. E. Dendy, 'Two methods of Galerkin type achieving optimum L^2 rates of convergences for first-order hyperbolics', *SIAM J. Numer. Anal.*, **11**, 637–653 (1974).
3. W. H. Raymond and A. Garder, 'Selective damping in a Galerkin method for solving wave problems with variable grids', *Mon. Weather Rev.*, **104**, 1583–1590 (1976).
4. T. J. R. Hughes and T. E. Tezduyar, 'Finite element methods for first-order hyperbolic systems with special emphasis on the compressible Euler equations', *Comput. Methods Appl. Mech. Eng.*, **45**, 217–283 (1984).
5. J. Donea, 'A Taylor–Galerkin method for convective transport problems', *Int. j. numer. methods eng.*, **20**, 101–119 (1984).
6. A. J. Baker and J. W. Kim, 'A Taylor weak statement algorithm for hyperbolic conservation laws', *Int. j. numer. methods fluids*, **7**, 489–520 (1987).
7. J. T. Oden, T. Strouboulis and P. Devloo, 'Adaptive finite element methods for the analysis of inviscid compressible flow: Part I. Fast refinement/unrefinement and moving mesh methods for unstructured meshes', *Comput. Methods Appl. Mech. Eng.*, **59**, 327–362 (1986).
8. A. Harten, 'High resolution schemes for hyperbolic conservation laws', *J. Comput. Phys.*, **49**, 357–393 (1983).
9. P. K. Sweby, 'High resolution schemes using flux limiters for hyperbolic conservation laws', *SIAM J. Numer. Anal.*, **21**, 995–1011 (1984).
10. P. Colella and P. R. Woodward, 'The piecewise-parabolic method (PPM) for gas-dynamical simulation', *J. Comput. Phys.*, **54**, 174–201 (1984).
11. S. Osher and S. Chakravarthy, 'High resolution schemes and the entropy condition', *SIAM J. Numer. Anal.*, **21**, 955–984 (1984).
12. H. C. Yee and A. Harten, 'Implicit TVD schemes for hyperbolic conservation laws in curvilinear coordinates', *AIAA J.*, **25**, 266–274 (1987).
13. J. Y. Yang, Y. Liu and H. Lomax, 'Computations of shock-wave reflection by circular cylinders', *AIAA J.*, **25**, 683–689 (1987).
14. A. Harten and S. Osher, 'Uniformly high order accurate non-oscillatory schemes, I', *SIAM J. Numer. Anal.*, **24**, 279–309 (1987).
15. A. Harten, B. Engquist, S. Osher and S. Chakravarthy, 'Uniformly high order accurate essentially nonoscillatory schemes, II', *J. Comput. Phys.*, **71**, 231 (1987).

16. A. Harten, S. Osher, B. Engquist and S. Chakravarthy, 'Uniformly high order accurate essentially non-oscillatory schemes, III', *J. Appl. Numer. Math.*, **2**, 347 (1986).
17. J. Y. Yang and C. K. Lombard, 'Uniformly second order ENO schemes for the Euler equations', *AIAA Paper 87-1166-CP*, 1987.
18. C. W. Shu, 'TVB uniformly high order schemes for conservation laws,' *Math. Comput.*, **49**, 105–121 (1987).
19. T. J. R. Hughes and M. Mallet, 'A high precision finite element method for shock-tube calculations', in R. H. Gallagher, G. F. Cavey, J. T. Oden and O. C. Zienkiewicz (eds), *Finite Elements in Fluids, Vol. 6*, Wiley, New York, 1985.
20. P. L. Roe, 'Approximate Riemann solvers, parameter vectors and difference schemes', *J. Comput. Phys.*, **43**, 357–372 (1981).
21. P. L. Roe, 'Some contributions to the modelling of discontinuous flows', Notes for a lecture presented to *AMS/SIAM Summer Seminar on Large Scale Computations in Fluid Mechanics*, Scripps Institute of Oceanography, University of California, San Diego, 26 June–8 July 1983.
22. K. W. Morton, 'Generalized Galerkin methods for hyperbolic problems', *Comput. Methods Appl. Mech. Eng.*, **52**, 847–871 (1985).
23. R. Löhner, K. Morgan, M. Vahdati, J. P. Boris and D. L. Book, 'FEM–FCT: combining unstructured grids with high resolution', *Commun. Appl. Numer. Methods*, **4**, 717–730 (1988).
24. R. Löhner, K. Morgan and O. C. Zienkiewicz, 'An adaptive finite element procedure for high speed flows', *Comput. Methods Appl. Mech. Eng.*, **51**, 441–465 (1985).
25. B. Cockburn, S. Y. Lin and C. W. Shu, 'TVB Runge–Kutta local projection discontinuous Galerkin finite element method for conservation laws III: One dimensional systems', *J. Comput. Phys.*, **84**, 90–113 (1989).
26. H. C. Yee, 'Upwind and symmetric shock-capturing schemes', *NASA TM 89464*, 1987.
27. P. L. Roe, 'Generalized formulation of TVD Lax–Wendroff schemes', *ICASE Report No. 84-53*, 1984.
28. S. F. Davis, 'TVD finite difference schemes and artificial viscosity', *ICASE Report No. 84-20*, 1984.
29. G. A. Sod, 'Survey of several finite difference methods for systems of nonlinear hyperbolic conservation laws', *J. Comput. Phys.*, **27**, 1–31 (1978).
30. P. Woodward and P. Colella, 'The numerical simulation of two-dimensional fluid flow with strong shocks', *J. Comput. Phys.*, **54**, 115–173 (1984).
31. T. J. R. Hughes and M. Mallet, 'A new finite element formulation for computational fluid dynamics. IV. A discontinuity capturing operator for multidimensional advective–diffusive system', *Comput. Methods Appl. Mech. Eng.*, **58**, 329–336 (1986).